Modelling the amorphous phase of a melt crystallized, semicrystalline polymer: segment distribution, chain stiffness, and deformation

Frans A. M. Leermakers and Jan M. H. M. Scheutjens
Laboratory for Physical and Colloid Chemistry, Agricultural University, De Dreijen 6, 6703 BC Wageningen, The Netherlands

and Richard J. Gaylord
The Polymer Group, Department of Metallurgy, University of Illinois at Urbana-Champaign, Urbana, Illinois 61801, USA
(Received 9 December 1983; revised 16 February 1984)

The analogy between the Gambler's Ruin problem and the statistics of loops and bridges in the amorphous region of lamellar semicrystalline polymers was first recognized by Guttman *et al.* Results for the loop and bridge distribution compare very well with recent data from Monte Carlo calculations. However, when the molecular weight of the polymer is low, a substantial part of the amorphous region is filled by cilia and free polymer. We examined their relative importance by adapting the matrix formalism developed by DiMarzio and Rubin. The Gambler's Ruin results are recovered for high molecular weight polymer. In addition it will be shown that the effect of the temperature (chain stiffness) can be simulated by rescaling the steplength of a random walk chain. Mean field theories incorporate segment–solvent interactions and allow for non-uniform segment densities by weighting each step according to the local concentrations. Using these weighting factors, we find deformation to be controlled by energetic interactions rather than by entropy. At large strain a 'necking' process occurs. However, in the presence of a good solvent, the material is soft and flexible.

(Keywords: amorphous polymer; semicrystalline polymer; polymer deformation; random walk statistics; mean field theory; gambler's ruin)

INTRODUCTION

A theoretical analysis of the properties of the amorphous component of a semicrystalline polymer must be based upon the recognition that the crystalline regions introduce surfaces which are impenetrable to the material residing within the amorphous regions. Four types of amorphous polymeric material can be identified: bridges, whose end segments are attached to opposing crystal surfaces; loops, whose end segments are attached to the same crystal surface; cilia, which have one end segment attached to a crystal surface and one unattached end segment; and floating chains, which have both end segments unattached. In 1975, Pettracone *et al.*[1] calculated the birefringence–strain behaviour of cilia, loops and bridges. In 1978 Lohse and Gaylord[2] calculated the modulus behaviour of all four chain types. The birefringence calculations were discrete and used both the matrix method of DiMarzio and Rubin[3] for a random walk on a cubic lattice and a Monte Carlo analysis for a random walk on a tetrahedral lattice incorporating the rotational isomeric state scheme. The modulus calculations were continuum and used the method of images[4,5] with the RIS scheme incorporated. None of the calculations considered segment–segment interactions or segment–crystal surface interactions and both treatments took the crystal surfaces to be mathematically absorbing barriers. In each paper, it was pointed out that the analyses were single chain analyses and that knowledge of the numbers and contour length distributions of the four chain types was needed in order to calculate the total behaviour of the amorphous regions.

These quantities clearly will depend on the crystallization process. Unfortunately, melt crystallization is a complex process which is not yet fully understood. There is however, one ideal situation: instantaneous crystallization. For this hypothetical process three profound insights have recently been made. The first insight, by Flory and Yoon[6], is that the topology of the chains in the original melt state must be conserved during the crystallization process. The second insight, by Guttman, DiMarzio and Hoffman[7,8], is that the numbers and contour lengths of each of the chain types in the final amorphous region can be determined by a consideration of the gambler's ruin with renewal problem. The third insight, by Rubin[9], is that a random walk between mathematically absorbing boundaries with renewal is equivalent to a random walk between reflecting boundaries. We will use these insights to analyse the amorphous region of an instantaneously melt crystallized semicrystalline polymer in detail.

0032-3861/84/111577-12$03.00

MATHEMATICAL PRELIMINARIES

Recently, two nearly identical lattice theories have been developed[10-12] which extend the DiMarzio and Rubin matrix formalism for ideal chains between a pair of parallel, impenetrable surfaces with segment–surface interaction[3], by incorporating segment–solvent interactions via a mean field analysis. We will give only a brief description of these theories here (for full details, see original papers[10-12]).

We define a lattice composed of layers $i=0, 1, 2, 3,\ldots,M, M+1$, each layer containing L lattice sites. The coordination number of lattice is z. We call the fraction of nearest neighbour lattice sites which are in the same layer λ_0 and the fractions which are in adjacent layers λ_{-1} and λ_1 (e.g., for a cubic lattice: $z=6$; $\lambda_0=2/3$; $\lambda_{-1}=\lambda_1=1/6$). In the lattice system we have n polymer chains, each having r segments and n^0 holes (or solvent molecules). Therefore

$$n^0+nr=ML \tag{1}$$

Rather than working with the actual number of polymers, we will work with the following volume fractions in each layer i:

$$\phi_i=n_i/L; \qquad \phi_i^0=n_i^0/L \tag{2}$$

where n_i and n_i^0 are the number of segments and holes, respectively, in layer i.

We first examine the chain statistics of the lattice system. A chain is built up by joining previously unattached monomer units, numbered $s=1,\ldots,r$. We start with a 'free segment' or monomer. The probability of finding this segment in layer i is given by the free segment probability p_i. A second segment must now be attached to the first one and therefore its location is restricted to either a preceding layer, a succeeding layer or the same layer as the first segment. The probabilities of this segment being in these locations are $\lambda_{-1}p(i,1)p_{i-1}$, $\lambda_1 p(i,1)p_{i+1}$ and $\lambda_0 p(i,1)p_i$, respectively. (Note: $p(i,1)=p_i$). We now define the end segment probability $p(i,2)$ as the probability of finding the end of a dimer in layer i. This quantity is given by:

$$p(i,2)=\{p(i-1,1)\lambda_{-1}+p(i,1)\lambda_0+p(i+1,1)\lambda_1\}p_i \tag{3}$$

Continuing this analysis for all r segments of the chain, we obtain $r-1$ recurrent relations having the general form:

$$p(i,s+1)=\{p(i-1,s)\lambda_{-1}+p(i,s)\lambda_0+p(i+1,s)\lambda_1\}p_i \tag{4}$$

to be performed for all layers i. These recurrent relations can be arranged in a matrix:

$$\underline{p}(s)=\underline{\underline{w}}\underline{p}(s-1) \tag{5}$$

So $\underline{\underline{w}}$ is a $M\times M$ tri-diagonal band matrix and $\underline{p}(s-1)$ and $\underline{p}(s)$ are vectors having M elements. We have introduced α and β in order to handle the boundary conditions. When $\alpha=\beta=0$ we have mathematically absorbing boundaries and thus no segments can physically reside in layers 0 or $M+1$. In this case the matrix is identical to that used by both Scheutjens and Fleer (SF) and Levine, Thomlinson and Robinson (LTR).

When $\alpha=1$ and $\beta=0$ there are mathematically reflecting boundaries situated midway between the layers 0–1 and $M-M+1$. (The $\alpha=0$ and $\beta=1$ case has reflecting boundaries located at layer 1 and M. We will not use this last condition in this paper). We note that the matrix formalism above allows both multiple occupancy of lattice sites and backfolding by chain segments.

We will now examine the free segment probability p_i. The value of p_i is given by the following relation:

$$p_i=A\phi_i^0 e^{\chi\langle\phi_i-\phi_i^0\rangle} \tag{7}$$

The quantity $\ln p_i$ is essentially a potential arising from the segments themselves. The ϕ_i^0 term in equation (7) is the fraction of sites in layer i that are not occupied by other segments. This is an entropic quantity. The exponent in equation (7) accounts for energetic quantities. They are weighting factors based on segment–hole interactions. In the SF theory, an averaging of the segment–hole interactions over the three consecutive layers is done and

$$\langle x_i\rangle=\lambda_{-1}x_{i-1}+\lambda_0 x_i+\lambda_1 x_{i+1} \tag{8}$$

In the LTR theory, no averaging is done and $\langle x_i\rangle=x_i\chi$ is the segment–hole interaction parameter defined by:

$$\chi=\frac{z}{kT}(\varepsilon^{op}-1/2(\varepsilon^{oo}+\varepsilon^{pp})) \tag{9}$$

ε stands for the gain or loss of enthalpy for various types of contacts in the system: pp = segment–segment; po = segment–hole; oo = hole–hole. The quantity A is a normalization constant (this will be discussed later). Starting with the free segment probability $p(i,1)=p_i$ we can calculate the end segment probability $p(i,s)$ using the recurrent relation (5). We than collect these probabilities in a matrix $\underline{\underline{p}}$:

$$\underline{\underline{p}}=\begin{vmatrix} p(1,1) & p(1,2) & \cdots & p(1,s) & \cdots & p(1,r) \\ & & & \vdots & & \\ p(i,1) & p(i,2) & & p(i,s) & & p(i,r) \\ & & & \vdots & & \\ p(M,1) & p(M,2) & \cdots & p(M,s) & \cdots & p(M,r) \end{vmatrix} \tag{10}$$

$$\begin{vmatrix} p(1,s) \\ p(2,s) \\ \cdot \\ p(i,s) \\ \cdot \\ p(M-1,s) \\ p(M,s) \end{vmatrix} = \begin{vmatrix} & (\lambda_0+\alpha\lambda_{-1})p_1 & (\lambda_1+\beta\lambda_{-1})p_1 \\ \lambda_{-1}p_2 & \lambda_0 p_2 & \lambda_1 p_2 \\ \cdot & \cdot & \cdot \\ \lambda_{-1}p_i & \lambda_0 p_i & \lambda_1 p_i \\ \cdot & \cdot & \cdot \\ \lambda_{-1}p_{M-1} & \lambda_0 p_{M-1} & \lambda_1 p_{M-1} \\ (\lambda_{-1}+\beta\lambda_1)p_M & (\lambda_0+\alpha\lambda_1)p_M & \end{vmatrix} \times \begin{bmatrix} p(1,s-1) \\ p(2,s-1) \\ \cdot \\ p(i,s-1) \\ \cdot \\ p(M-1,s-1) \\ p(M,s-1) \end{bmatrix} \tag{6}$$

The elements of matrix $\underline{p}$ provide all of the information necessary to calculate the properties of the system. The density profile made up by the chains in the system is determined using the general composition formula[10]:

$$\phi_i = B(1/p_i)\sum_{s=1}^{r} p(i,s)p(i,r-s+1) \qquad (1)$$

where B is a normalization constant. The $p(i,s)$ and $p(i,r-s+1)$ quantities represent two connected subchains. The divisor p_i is present because the subchains share one overlapping segment. After determining the total segment density profile of all the chains in the system we then recalculate the free segment probability using equation (7). We perform this computation iteratively, until a self consistent density profile is obtained (i.e. until resubstitution of a ϕ_i produces the same value of ϕ_i). This defines the equilibrium state of the system.

MODELLING THE AMORPHOUS PHASE OF A MELT CRYSTALLIZED POLYMER

As stated in the introduction, for the instantaneous melt crystallization process proposed by Flory and Yoon[6], Guttman *et al.*[7,8] have used the results of the classical gambler's ruin with infinite renewal problem to calculate the numbers and contour length distribution of bridges and loops formed in the amorphous regions of the semicrystalline polymer. Their calculations apply only to a system of infinitely long chains. We will use the matrix method described above to extend the gambler's ruin analysis to a system of finite chains.

First we examine the initial melt state, in which the density is constant. Then the volume fractions in every layer are: $\phi_i = \phi_* = nr/ML$ and $\phi_i^0 = 1-\phi_*$. Using the following normalization for p_i in equation (7):

$$1/A = (1-\phi_*)e^{\chi(2\phi_*-1)} \qquad (12)$$

then produces a free segment probability $p_i = 1$ for all i. This means that all of the segments 'feel' the same potential at each position in the system. We now use the matrix method. We assign reflecting boundary conditions ($\alpha=1$, $\beta=0$) with this starting vector: $p(i,1)=p_i=1$ for all i.

Because of the reflecting character of the boundaries, the segments do not feel any physical boundary, and therefore the segments will have no preferential direction to go. Mathematically we observe that $p(i,s)$ is equal to 1 for all i, s.

So,

$$p(r) = \sum_{i=1}^{M} p(i,r) = \sum_{i=1}^{M} p(i,s) = M$$

showing that the probability of finding any segment between the boundaries is equal. The density can be calculated with the following composition formula:

$$\phi_i = \frac{n}{Lp(r)p_i}\sum_{s=1}^{r} p(i,s)p(i,r-s+1) \qquad (13)$$

While the normalization $n/Lp(r)$ is ϕ_*/r, i.e. the contribution of one segment to an average density. The result is a constant density $\phi_i = \phi_*$ for all i and no iterations are necessary.

This lattice result is in agreement with the continuum analysis of a floating chain between reflecting boundaries[13].

Now we examine the polymer just before crystallization. It is assumed that the melt will crystallize in the layers $i<1$ and $i>M$ with no movement of the chains in the amorphous region during the crystallization process. Thus, the constant density feature greatly simplifies our calculations of the contour length distributions of the chain parts in the amorphous region, which are illustrated in *Figure 1*.

In order to examine the chain parts in this region, one quantity that must be known is the so-called free chain probability. This is the probability of finding a chain which has all of its segments between layer 0 and $M+1$ and none of its segments in those 2 layers. This quantity is calculated by placing mathematically absorbing boundaries on 0 and $M+1$. Mathematically, we set $\alpha=\beta=0$ in equation (5). The free chain can start in any layer other than 0 and $M+1$ and so the following starting vector is used: $\underline{p}^f(1)^T = (1,1,\ldots,1)$. (We use the same normalization for p_i as given in equation (12)). Performing $r-1$ matrix multiplications of equation (5) yields a matrix containing $p^f(i,s)$ elements ($i=1,\ldots,M$; $s=1,\ldots,r$):

$$\underline{p}^f = \begin{vmatrix} 1 & p^f(1,2) & \cdots & p^f(1,s) & \cdots & p^f(1,r) \\ 1 & 1 & \cdots & p^f(2,s) & \cdots & p^f(2,r) \\ \cdot & \cdot & \cdots & \cdot & \cdots & \cdot \\ 1 & 1 & \cdots & p^f(i,s) & \cdots & p^f(i,r) \\ \cdot & \cdot & \cdots & \cdot & \cdots & \cdot \\ 1 & 1 & \cdots & p^f(M-1,s) & \cdots & p^f(M-1,r) \\ 1 & p^f(M,2) & \cdots & p^f(M,s) & \cdots & p^f(M,r) \end{vmatrix} \qquad (14)$$

The number of free chains is given by the probability ($\sum_{i=1}^{M} p^f(i,r)$) of finding a free chain between layer 0 and $M+1$ divided by the probability of finding any chain in this region multiplied by the number of chains in this region:

$$n^{free} = n\sum_{i=1}^{M} p^f(i,r) \Big/ \sum_{i=1}^{M} p(i,r) = p^f(r)n/M \qquad (15)$$

The number of cilia of length s is equal to twice the probability of finding a free chain end of length s ending in layer 1 times the probability of passing the boundary λ_{-1}

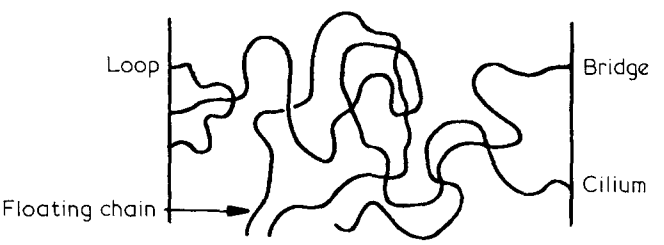

Figure 1 Chain parts between two boundaries

multiplied by n/M. There is a factor of two because there are two chain ends. Mathematically,

$$n_s^{\text{cilia}} = p^{\text{f}}(1,s)\lambda_1 2n/M \tag{16}$$

The numbers of loops and bridges having length s, is calculated by determining the probability of finding a chain part starting in layer 1 and being in either layer 1 or M after s steps.

The starting vector $p^{\text{c}}(1)^T=(1,0,0,\ldots,0)$ accounts for the fact that the first segment is in layer 1 (c=cilium). Performing the matrix multiplications of equation (5) while $\alpha=\beta=0$, gives end segment probability matrix $\underline{\underline{p}}^{\text{c}}$:

$$\underline{\underline{p}}^{\text{c}} = \begin{vmatrix} 1 & p^{\text{c}}(1,2) & \cdots & p^{\text{c}}(1,s) & \cdots & p^{\text{c}}(1,r) \\ 0 & p^{\text{c}}(2,2) & \cdots & p^{\text{c}}(2,s) & \cdots & p^{\text{c}}(2,r) \\ \cdot & \cdot & \cdots & \cdot & \cdots & \cdot \\ 0 & 0 & \cdots & p^{\text{c}}(i,s) & \cdots & p^{\text{c}}(i,s) \\ \cdot & \cdot & \cdots & \cdot & \cdots & \cdot \\ 0 & 0 & \cdots & p^{\text{c}}(M,s) & \cdots & p^{\text{c}}(M,\text{r}) \end{vmatrix} \tag{17}$$

Only the first and last row are needed in order to calculate the number of loops and bridges of length s.

$$n_s^{\text{loop}} = p^{\text{c}}(1,s)\lambda_{-1}\lambda_1(r-s-1)\frac{n}{M} \tag{18}$$

$$n_s^{\text{bridge}} = p^{\text{c}}(M,s)\lambda_{-1}\lambda_{-1}(r-s-1)\frac{n}{M} \tag{19}$$

where the $r-s-1$ terms represent the number of ways of forming a loop or a bridge having s segments from a chain consisting of $r-2$ segments. (2 extra segments are needed for both ends of a loop or bridge). A loop or bridge of s segments is passing the boundary between layer 0–1 with its 0th segment (probability is λ_{-1}) and its $s+1$th segment is passing the boundary 1–0 (λ_1) respectively $M-M+1$ (λ_{-1}). The boundary between layer $M-M+1$ will produce a same number of loops, bridges and cilia. So the total number of loops, bridges and cilia are twice the numerical values as given in equations(16, 18, 19). SF calculate their chain part distributions for an arbitrary density profile. Their results reduce to ours when a flat density profile is used.

We now examine the final semicrystalline state. After crystallization we have real, impenetrable crystal surfaces in layer 0 and $M+1$ and a system of permanent loops, bridges, cilia and floating chains between mathematically absorbing barriers. These chains have the same contour length distributions previously calculated for loops, bridges, cilia and free chains respectively, between reflecting boundaries. In order to calculate the volume fractions of these permanent chain species, the following end segment probabilities must be known:

(1) The end segment probabilities of a chain having its first segment adsorbed at a surface. We use the starting vector $\underline{p}^{\text{c}}(1)^T=(p_1,0,0,\ldots)$ and perform $r-1$ matrix multiplications of equation (5) with $\alpha=\beta=0$ to get the $p^{\text{c}}(i,s)$ matrix.

(2) The end segment probabilities of a floating chain, $p^{\text{f}}(i,s)$. This is calculated using the starting vector $p^{\text{f}}(i,1)=p_i$ for all i and also absorbing boundary conditions. We collect the results of the matrix procedure in the matrix $p^{\text{f}}(i,s)$.

Using the $\underline{\underline{p}}^{\text{c}}$ and $\underline{\underline{p}}^{\text{f}}$ matrices, we calculate the volume fractions of the various chain types from the following relations:

$$\phi_i^{\text{float}} = n^{\text{free}}/(Lp^{\text{f}}(r)p_i)\sum_{s=1}^{r} p^{\text{f}}(i,s)p^{\text{f}}(i,r-s+1) \tag{20}$$

$$\phi_i^{\text{cilia}} = \sum_{s=1}^{r-1}\{n_s^{\text{cilia}}/(Lp^{\text{c}}(s)p_i) \times \sum_{k=1}^{s}[p^{\text{c}}(i,k)p^{\text{f}}(i,s-k+1)]\} \tag{21}$$

$$\phi_i^{\text{loop}} = \sum_{s=1}^{r-2}\{n_s^{\text{loop}}/(Lp^{\text{c}}(1,s)p_i) \times \sum_{k=1}^{s}[p^{\text{c}}(i,k)p^{\text{c}}(i,s-k+1)]\} \tag{22}$$

$$\phi_i^{\text{bridge}} = \sum_{s=M}^{r-2}\{n_s^{\text{bridge}}/(Lp^{\text{c}}(M,s)p_i) \times \sum_{k=1}^{s}[p^{\text{c}}(i,k)p^{\text{c}}(M-i+1,s-k+1)]\} \tag{23}$$

where

$$p^{\text{c}}(s)=\sum_{i=1}^{M} p^{\text{c}}(i,s) \quad \text{and} \quad p^{\text{f}}(r)=\sum_{i=1}^{M} p^{\text{f}}(i,r) \tag{24}$$

From equations (21–23) we can calculate the total segment density profile of the loops, bridges and cilia emanating from the surface situated at layer 0. The loops, bridges and cilia emanating from the other surface will display a total density profile which is a mirror image (with respect to a plane of symmetry midway between the two walls) of the calculated profile. The two profiles added together with the profile calculated for floating chains will then give the total density profile of the amorphous region of the semicrystalline polymer (see *Figure 4*). Equation (7) implicitly assumes that there is no energetic difference between a segment-crystal and a segment-segment contact. This is reasonable when both regions are comprised of the same sort of segments and the densities of the crystalline and the amorphous regions are not too disparate. The use of equation (7) does indeed produce a constant self consistent density profile when the computer calculations are performed and again, no iterations are necessary.

CHAIN STIFFNESS EFFECTS

Temperature effects can readily be studied once chain stiffness is introduced into the matrix formulation. This can be done in the manner suggested by Rubin and DiMarzio[3]. We will illustrate the procedure for the case of a cubic lattice system, using a modified form of equation (5) and referring to *Figure 2*.

In the flexible chain case, it suffices to know the position of segment s in layer i in order to calculate the position of segment $s+1$ (see equation (3)). However, incorporation of stiffness requires reference to an additional segment $(s-1)$. The M component vector $\underline{p}$ in equation (5) then becomes a $6M$ component vector. A typical end segment

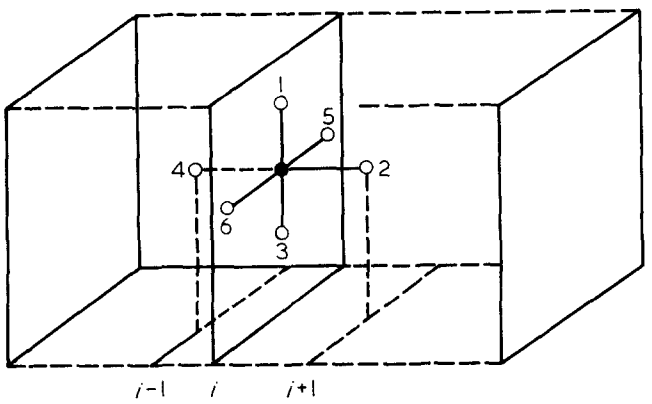

Figure 2 Orientations of 3 successive segments on a cubic lattice

probability vector can be written as $p(i,j,s)$ where $i=1,\ldots,M$; $j=1,\ldots,6$ and $s=1,\ldots,r$. In words it gives the probability of finding the end of a s-mer in layer i, while its previous segment $(s-1)$ is in the $-j$ direction. (If $j=4$, then $-i=2$).

The λ_0, λ_1 and λ_{-1} elements of the transition matrix equation (5) are replaced by the following submatrices:

$$\lambda_{-1}=\begin{vmatrix} 0 & 0 & 0 & 0 & 0 & 0 \\ L & S & L & B & L & L \\ 0 & 0 & 0 & 0 & 0 & 0 \\ 0 & 0 & 0 & 0 & 0 & 0 \\ 0 & 0 & 0 & 0 & 0 & 0 \\ 0 & 0 & 0 & 0 & 0 & 0 \end{vmatrix}$$

$$\lambda_0=\begin{vmatrix} S & L & B & L & L & L \\ 0 & 0 & 0 & 0 & 0 & 0 \\ B & L & S & L & L & L \\ 0 & 0 & 0 & 0 & 0 & 0 \\ L & L & L & L & S & B \\ L & L & L & L & B & S \end{vmatrix}$$

$$\lambda_1=\begin{vmatrix} 0 & 0 & 0 & 0 & 0 & 0 \\ 0 & 0 & 0 & 0 & 0 & 0 \\ 0 & 0 & 0 & 0 & 0 & 0 \\ L & B & L & S & L & L \\ 0 & 0 & 0 & 0 & 0 & 0 \\ 0 & 0 & 0 & 0 & 0 & 0 \end{vmatrix} \qquad (25)$$

Referring to *Figure 2*, the quantities L, S and B are the probabilities of a segment being oriented at an angle of 90°, 180° and 0° respectively, with respect to the preceding two segments. These probabilities are given by:

$$S=s(4l+s+b) \qquad L=l/(4l+b+s)$$
$$\text{and} \quad B=b/(4l+s+b) \qquad (26)$$

where s, l and b are Boltzmann weighting factors:

$$s=\exp(-\varepsilon^s/kT), \qquad l=\exp(-\varepsilon^l/kT),$$
$$b=\exp(-\varepsilon^b/kT) \qquad (27)$$

and $\varepsilon^l, \varepsilon^s, \varepsilon^b$ are the appropriate energies associated with L, S, B conformation.

Now that our transition matrix is defined, we can calculate the conformational properties of chains incorporating short range interactions. To illustrate the procedure we will calculate the density profile of the melt again. Using the starting vector $p(i,j,1)=p_i/6$ for $i=1,\ldots,M$ and $j=1,\ldots,6$, the calculation of the end segment probabilities requires $r-1$ matrix multiplications (with reflecting boundary conditions) of equation (5), with equation (25) replacing the λ quantities therein. However, since stiffness is only defined by the location of three consecutive segments, the first matrix multiplication uses $L=B=S=1/6$, while the remaining $r-2$ multiplications use the L, B, S as given in equation (26). In order to use the end segment probabilities in the volume fraction calculation, it is necessary to devise a composition law for the connection of the s and the $r-s+1$ subchains from which the entire r chain is formed. In general for a semiflexible chain, it is necessary that there be an accounting of the energetics for the orientation of the segment s and $r-s+1$ with respect to one another. This is accomplished by using the following matrix multiplication:

$$\underline{p}'(s)=\underline{\underline{w}}'\underline{p}(s) \qquad (28)$$

where $\underline{\underline{w}}'$ is a $M\times M$ matrix having all zero off diagonal elements and having diagonal elements comprised of the following submatrix:

$$\underline{\underline{w}}'_{sub}=\begin{vmatrix} B & L & S & L & L & L \\ L & B & L & S & L & L \\ S & L & B & L & L & L \\ L & S & L & B & L & L \\ L & L & L & L & B & S \\ L & L & L & L & S & B \end{vmatrix} \qquad (29)$$

A component of $p'(s)$, $p'(i,j,s)$, is the probability of finding the end of a s-mer in layer i and that a next segment will go in the j direction. We note that in equation (29) the quantities B are located on the diagonal in contrast to their locations in equation (25). This is a result of the fact that, if there is a joining of two subchains shch that the last segment of the s subchain and the first segment of the $r-s+1$ subchain both 'come from' the jth direction, there must be an associated backfolding energy. As soon as the first or the last segment of the chain is involved in the composition we have to use a flexible connection. Analogous to the modification in equation (25) we have to use $L=B=S=1/6$ in equation (29) in this case.

The density profile of melt is given by:

$$\phi_i=n/(Lp(r)p_i)\sum_{s=1}^{r}\sum_{j=1}^{6}p'(i,j,p(i,j,r-s+1) \qquad (30)$$

(Naturally, when $s=1, r$ the elements of $\underline{\underline{w}}'$ are all equal to 1/6 as discussed above).

It is clear that we can incorporate stiffness into the gambler's ruin analysis of the melt state. Following the derivation above, we need two end segment probability matrices.

(1) The end segment probabilities of a chain starting in layer 1 which have a previous segment in layer 0. In this

case, the starting vector is $\underline{p}^c(1)$, with $\underline{p}^c(i,j,1)=0$ for all i and j except $p^c(1,2,1)=1/6$. Since we know that there is a segment in the crystal, we do not have any flexible chain elements. The results are collected in $\underline{\underline{p}}^c$.

(2) The end segment probabilities of a chain who does not pass any boundary. This quantity is found using the starting vector: $\underline{p}^f(1)$, $p^f(i,j,1)=1/6$ for $i=1,\ldots,M$, $j=1,\ldots,6$ using the absorbing boundary conditions. We collect the results in $\underline{\underline{p}}^f$.

$$n^{\text{free}}=p^f(r)n/M \tag{31}$$

$$n_s^{\text{cilia}}=p^{f'}(1,2,s)2n/M \tag{32}$$

$$n_s^{\text{loop}}=p^{c'}(1,2,s)(r-s-1)n/M \tag{33}$$

$$n_s^{\text{bridge}}=p^{c'}(M,4,s)(r-s-1)n/M \tag{34}$$

where

$$p^f(r)=\sum_{i=1}^{M}\sum_{j=1}^{6}p^f(i,j,r)$$

We note that there are no λ terms in these expressions because they have been replaced by the use of the connection formula of equation (28). Again we have only calculated the chains emanating from the wall between layer 0–1; an equal number of loops, bridges and cilia will emanate from the wall between layers $M-M+1$.

The calculation of the volume fractions of cilia, loops, bridges and floating chains are analogous to the melt calculation just given. To find the adsorbed end segment probabilities, we use the starting vector $p^c(1)$, $p^c(i,j,1)=0$ for all i,j except for the $p^c(1,2,1)$ element which equals p_1. Since there is actually a segment in the crystal, all of the $r-1$ matrix multiplications of equation (5) (with equation (25) substituted for the λ terms), use the L,S,B values given in equation (26). The end segment probabilities of these chain types are denoted by $p^c(i,j,s)$. Secondly, we need the free end segment probabilities for chains which are not passing the boundaries. Using the adsorbing boundary conditions and the starting vector $\underline{p}^f(1)$, $p^f(i,j,1)=p_i/6$ for $i=1,\ldots,M$ and $j=1,\ldots,6$ we end up with the free end segment probability matrix $\underline{\underline{p}}^f$.

The volume fraction formulas for the different chain species are:

$$\phi_i^{\text{float}}=n^{\text{free}}/(Lp^f(r)p_i)\times\sum_{s=1}^{r}\sum_{j=1}^{6}p^{f'}(i,j,s)p^f(i,j,r-s+1) \tag{35}$$

$$\phi_i^{\text{loop}}=\sum_{s=1}^{r-2}\{n_s^{\text{loop}}/(Lp^{c'}(1,2,s)p_i)\times\sum_{k=1}^{s}\sum_{j=1}^{6}[p^{c'}(i,j,s)p^c(i,j,k-s+1)]\} \tag{36}$$

$$\phi_i^{\text{bridge}}=\sum_{s=M}^{r-2}\{n_s^{\text{bridge}}/Lp^{c'}(M,4,s)p_i)\times\sum_{k=1}^{s}\sum_{j=1}^{6}[p^{c'}(i,j,s)p^c(M-i+1,-j,k-s+1)]\} \tag{37}$$

$$\phi_i^{\text{cilia}}=\sum_{s=1}^{r-1}\{n_s^{\text{cilia}}/(Lp^{c'}(s)p_i)\times\sum_{k=1}^{s}\sum_{j=1}^{6}[p^{c'}(i,j,s)p^f(i,j,k-s+1)]\} \tag{38}$$

where

$$p^{c'}(s)=\sum_{i=1}^{M}\sum_{j=1}^{6}p^{c'}(i,j,s)$$

The prime symbol is used above to indicate the use of equation (28). We note that in the case of a cilium, the $k=s$ term in equation (38) uses $B=L=S=1/6$, since one chain end is not fixed.

After recalculating the density of the amorphous phase, the density is proven to be consistent without the need for iterations.

RESULTS

In this section we present a selection of the numerical results. All of the calculations we will discuss were performed using a cubic lattice ($\lambda_0=2/3$, $\lambda_{-1}=\lambda_1=1/6$).

We first focus our attention on the flexible chain case. *Figure 3* gives the fraction of segments in loops, bridges, cilia and floating chains, as a function of the degree of polymerization r. Even for $r=3000$ the cilia are still very important (contribution of 20%). The limiting value of their average length is already reached and appears to be

$$\langle\text{cilium}\rangle=(M+1)(M+2)/2 \tag{39}$$

The fraction of end segments is $2/r$, so the limiting fraction of segments in cilia is $(M+1)(M+2)/r$. Therefore, r must be greater than $100(M+1)(M+2)$ before cilia contribute less than 1% to the amorphous region (if $M=20$, then $r>40\,000$).

The limiting formula for the probabilities p^{loop} and p^{bridge} of finding a loop or a bridge, respectively, are derived by Guttman *et al.*[8], via a gambler's ruin analysis. They also give the limiting values for the average loop and tail size, expressed in number of steps. The same values expressed in number of segments are one less and given by

$$\langle\text{loop}\rangle=2M+1 \tag{40}$$

$$\langle\text{bridge}\rangle=M^2+2M \tag{41}$$

Our computations for $r=25\,000$ show a deviation of less than 0.5% from these predictions. Qualitatively, equations (40) and (41) are supported by Monte Carlo

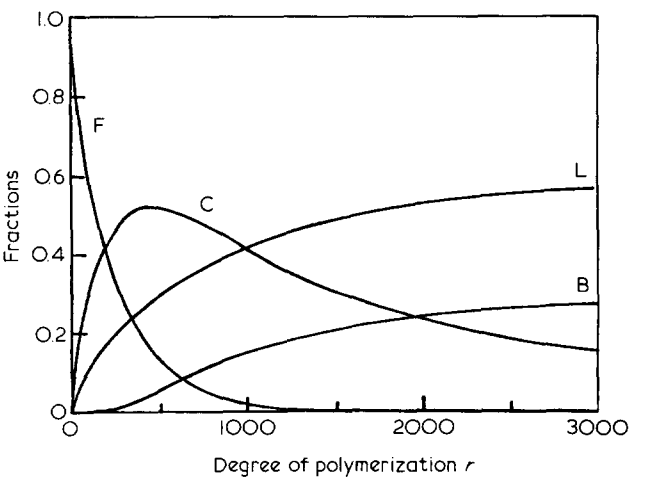

Figure 3 Fraction of segments in F=floating chains, C=cilia, L=loops, B=bridges, as a function of the degree of polymerization in the original melt. The wall distance $M=20$

calculations[14,15]. The duration of any walk is in agreement with Guttman *et. al.*[8]:

$$\bar{r}=3M \tag{42}$$

For smaller degrees of polymerization, bridges become less important. In particular when $r<M^2$, bridges will not contribute anymore to the amorphous phase. Alternatively, loops do contribute significantly even for $r<M$. This is due to the fact that most loops are very small, as we will see.

Figure 3 also shows the behaviour of cilia. The fraction of segments in cilia goes through a maximum where r is in the order of M^2. At this point, the cilia are the dominant chain species in the amorphous region, using up about 50% of all the segments in the amorphous phase. At very small r, the floating chains are the most prevalent chain species but as r increases their presence decreases rapidly and when $r>2M^2$ there are no floating chains left. We note that the M^2 dependences stated above are a result of the random coil character of the chains.

Figure 4 shows the calculated density profile of the amorphous region for $M=20$, $r=400$. We see that the floating chains are located primarily in the centre of the system (in contrast to the supposition of Pettracone *et al.*[1]), while the loops stay close to the walls. The bridges have a higher density near the centre of the system and the cilia are not very close to the walls. Clearly, the total density profile is constant.

Figure 5 gives the distribution of the chain lengths of the species making up the density profile of *Figure 4*. Note the multiplication factors in *Figure 5* for the different chain species. Because of the relatively small degree of polymerization, bridges are almost absent from the system. The bridges are very long as is shown and they have a rather symmetric distribution on the (log) plot of *Figure 5*. Instead, there are a great number of tight loops. Loops only 1 segment long make up about 20% of the total number of loops. This remarkable effect is also observed by Guttman, DiMarzio and Hoffman (GDH). The number of cilia is limited to 2 per chain. They are, however, longer than the loops, but not as long as bridges. Their distribution is very broad.

We now examine temperature effects on the composition of the amorphous phase by incorporating the stiffness effects into the chain. We presume different crystallization temperatures T_0 for a given hypothetical polymer. In all cases, we will use $B=0$, so that the probability of segment backfolding is zero. Only the energy difference $\Delta\varepsilon=(\varepsilon^s-\varepsilon^t)$ is relevant for the probability of an *L*-shape or an *S*-shape conformation.

$$S=\frac{1}{1+4e^{\Delta\varepsilon/kT_0}}; \qquad L=\frac{1}{4+e^{-\Delta\varepsilon/kT_0}} \tag{43}$$

Let us first choose $T_0=\infty$. This is equivalent to $\Delta\varepsilon=0$ which is similar to the flexible chain case except that backfolding is prohibited. *Figure 5* shows the length distribution of the loops, bridges and cilia.

We first compare the no backfolding case with the flexible case. Of course, one-segment loops do not occur when backfolding is prohibited but it is remarkable that the only effect of $B=0$ is to shift the loop distribution by about one segment without altering the shape of the curve. Even more interesting are the differences in the cilium and bridge length distributions. The average lengths of the bridges are about the same, or a bit smaller, but their numbers are three times greater. There are also more (short) cilia. Furthermore, the number of floating chains decreases about 50% (not shown in *Figure 5*). These effects are rather dramatic in nature, showing that backfolding does influence the lattice calculations in many cases. However, rescaling of the system largely compensates these effects as will be discussed below (*Figure 6*).

Figure 6 is a plot of the fraction of segments in loops, bridges, cilia and floating chains as a function of the logarithm of the absolute temperatures before crystallization for the case of $\Delta\varepsilon/k=300$ K and for some combinations of r and M. The actual choice of $\Delta\varepsilon$ is not important, and will not alter the shapes of the curves in *Figure 6*. A change in $\Delta\varepsilon$ will only cause a translation on the temperature axes. We see at least three distinct regimes in *Figure 6*.

(1) $T_0<T^*$ (see *Figure 6a*).

The results in this regime are lattice dependent artefacts. We will therefore not discuss this except to say that the results are predictable: 2/3 of the chains are floating

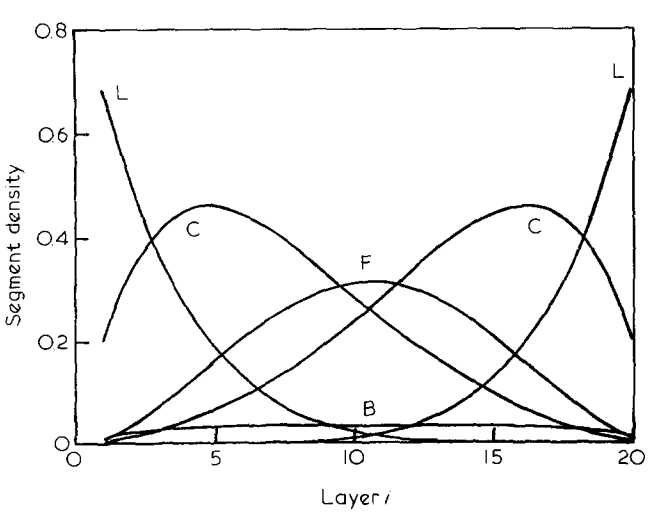

Figure 4 Density profiles for the chain species: L=loop, C=cilia, F=floating chains, B=bridge. The degree of polymerization of the original melt was $r=400$ and the wall distance $M=20$

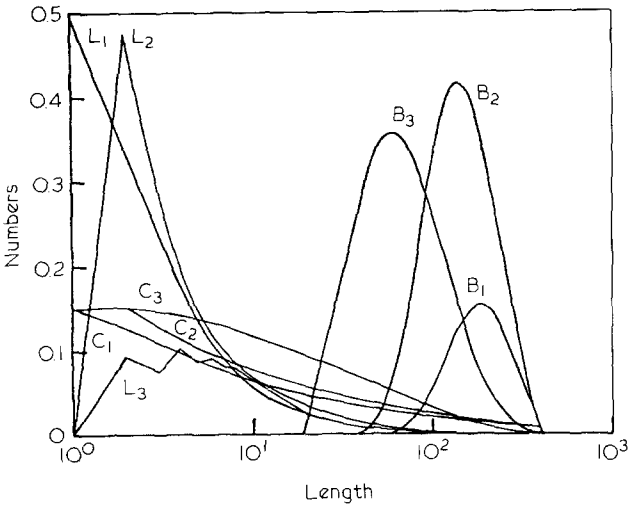

Figure 5 Distribution of lengths of L=loops, B=bridges, C=cilia. For 1, flexible chains; 2, no backfolding; 3, stiff chains ($\Delta\varepsilon/k=300$ K and $T_0=150$ K) $r=400$, $M=20$. Multiplication factors used: loops: 10×, bridges {(B_1 and B_2): 10^4×; B_3: 10^3×}, cilia: 10^2×

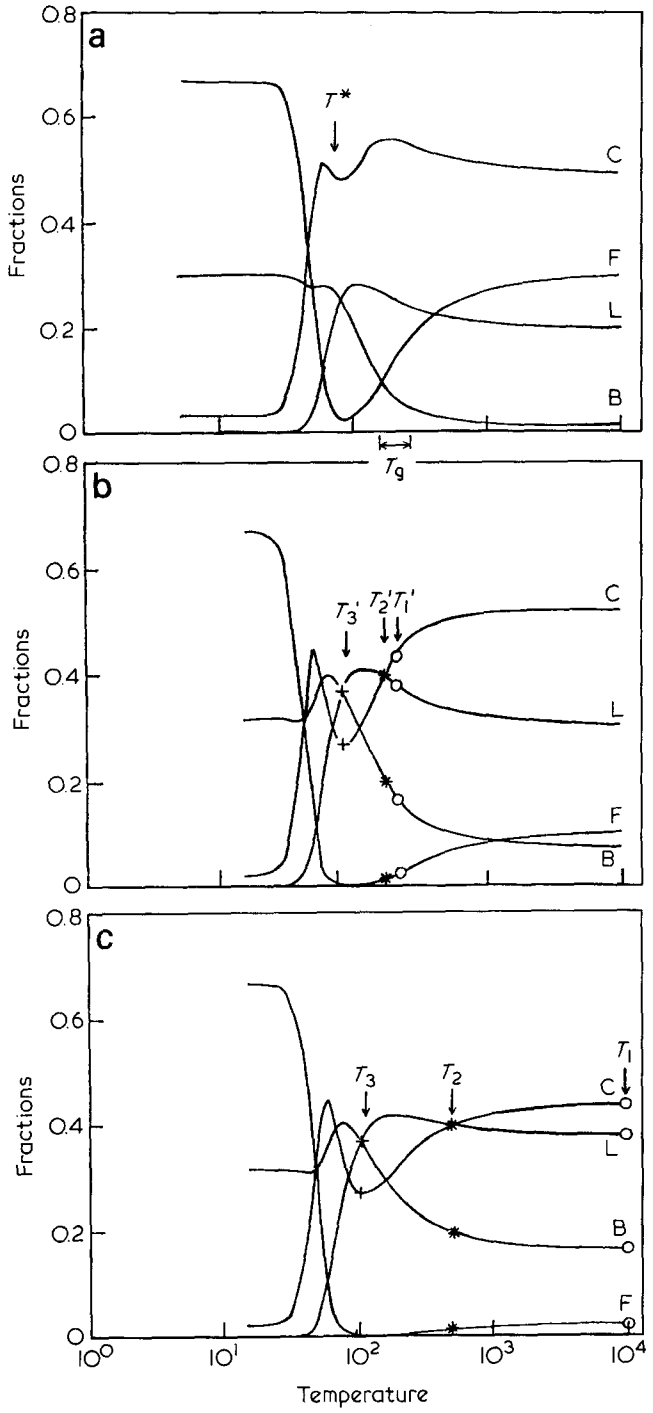

Figure 6 Fraction of segments in: C=cilia; F=floating chains; L=loops; B=bridges as a function of the crystallization temperature (Kelvin). $(\Delta\varepsilon/k)=300$ K. (a) $M=20$, $r=200$; (b) $M=10$, $r=200$; (c) $M=20$, $r=400$

chains parallel to the surface while the rest are bridges and (a small number of) cilia.

(2) $T^* < T_0 < T_g$

The next temperature which is relevant is the glass transition temperature $T_g \simeq \frac{1}{2}\Delta\varepsilon/k$. Below this temperature, chains cannot rearrange and as a result they will not be able to adopt the predicted equilibrium chain distribution of the gambler's ruin analysis. Therefore in this temperature range, our results are not meaningful.

(3) $T_0 > T_g$ is the temperature range which is relevant in practice. Starting from T^* we observe that floating chains will be more prevalent when the temperature before crystallization is higher. Near T^* there are almost no floating chains due to the expanded dimensions of random coils at lower temperature. Similarly, it is expected that the fraction of bridges will be lower when this temperature increases. The loops and cilia do show more remarkable effects. This can be explained with the help of *Figure 5*. In this Figure, the distribution of loops, bridges, cilia and floating chains is given for T_0 near $T^*(T_0=150\,\text{K}, \Delta\varepsilon/k=300\,\text{K})$. The average loop length is twice the length at $T_0\rightarrow\infty$. In particular there is a fivefold decrease in the number of small loops. We observe an oscillation in number of small loops of length less than ten. As expected, we see a big difference in the bridge behaviour at $T_0=150\,\text{K}$ as compared with $T_0\rightarrow\infty$. Bridges are 10 × more abundant, and their average length is smaller.

Returning to *Figure 6* we now can explain the maximum in the fraction of segments in loops at $T_0\cong 100\,\text{K}$. Two antagonistic effects, growth in the average length of loops and lowering of the numbers of loops, are acting simultaneously. The cilia behave differently because the total number of cilia is fixed at two whilst the average length of a cilium can differ as a function of temperature. The way this happens is dependent on the degree of polymerization. As shown in *Figure 6a* the cilia fraction goes through a maximum at $T_0\approx 200\,\text{K}$. However, when $r>400$ this maximum is not present and the fraction of cilia is a continuous growing function of the crystallization temperature. The maximum found for cilia for $r<400$ is in agreement with the results of *Figure 3*, where a maximum for the cilia fraction was also found. The following discussion about rescaling the system will make this behaviour more understandable. *Figures 6b* and *6c* show curves which are similar to *Figure 6a*. The system in *Figure 6c* ($M=20, r=400$) is twice as big as that in *Figure 6b* ($M=10, r=200$). *Figures 6b* and *6c* illustrate the principle that a system of nonflexible chains can be rescaled to a smaller system of more flexible chains. T_1-T_1', T_2-T_2', T_3-T_3' are typical examples where both systems have identical fractions of segments in loops, bridges, cilia and floating chains. Also the profiles of those chain species at corresponding temperatures (T_1-T_1' etc.) are similar (not indicated in the Figure). This rescaling phenomena agrees with observations of Guttman *et al.*[15].

Finally, we note that polydispersity is simulated by a super-position of different monodisperse chain length calculations. The results can therefore be discussed using *Figure 3*. During the instantaneous crystallization, a longer chain will be passing a boundary more often than does a small chain (and therefore will be divided into loops, bridges or cilia). The result is that floating chains, if present in the amorphous phase, will be short.

In the following subsections we will examine the properties of the amorphous phase as discussed above in more detail. Bond orientation and deformation will be discussed.

CALCULATION OF BIREFRINGENCE AND DIELECTRIC PROPERTIES

The calculation of the optical and electrical characteristics of the chains in the amorphous regions of the melt crystallized semicrystalline polymer requires knowledge of the orientation of the segments of the confined chains.

The matrix formulation we are using provides the necessary information quite readily. We can show the general procedure for floating chains here. The total number of segment–segment bonds is $(r-1)n/L$. A bond parallel to the plane is found when two adjacent segments are in a same layer:

$$\phi_i^{par} = \frac{n\lambda_0}{Lp(r)} \sum_{s=1}^{r-1} p(i,s)p(i,r-s) \tag{44}$$

The fraction of segments parallel and perpendicular is measured by birefringence and calculated by:

$$f^{par} = \frac{L}{n(r-1)} \sum_{i=1}^{M} \phi_i^{par} \tag{45}$$

$$f^{per} = 1 - f^{par} \tag{46}$$

So

$$f^{par} = \frac{\lambda_0}{(r-1)p(r)} \sum_{i=1}^{M} \sum_{s=1}^{r-1} p(i,s)p(i,r-s) \tag{47}$$

There seems to be an influence of the lattice in equation (47), since λ_0 is in this equation. For instance, for cubic lattices $\lambda_0 = 2/3$ and for hexagonal lattices $\lambda_0 = 1/2$. The latter one has no orthogonal bonds, and therefore f^{par} as given by equation (47) and f^{per} from equation (46) can be corrected by decomposition into real parallel and perpendicular parts to fit experimental quantities. It is simple to show that for isotropic lattices the result will be lattice independent.

CALCULATION OF DEFORMATION PROPERTIES

The theoretical model that we are using can be used to examine the role of the amorphous component of a semicrystalline polymer in the overall stress–strain behaviour of the material. We can model several very interesting reversible and irreversible deformation processes with our method. Both types of processes will result in a change in both the overall density and the density profile of the amorphous region as the surface separation is changed, depending on the value of the χ parameter. In a reversible deformation process, this may occur as a result of the migration of floating chains from between a pair of crystal lamellae, which are being brought together by the deformation, to between a pair of crystal lamellae which are being separated by the deformation. In this case, we have an open system for the floating chains which affects the free energy. (We will come back to this point later). In an irreversible deformation process, this may occur as a result of taut bridges either increasing their contour length by pulling segments out of the crystalline regions to which they are attached or by breaking into cilia (the break occurring either at the crystal surfaces or randomly along the bridge's contour length). The irreversible process can result in hysteretic stress–strain behaviour, such as Mullins effect, permanent set or even in failure via crack and craze propagation.

We must, however, be cautious in our analysis of the deformation behaviour of our system because:

(1) We cannot pinpoint the exact locations of the end segments of loops and bridges in our treatment.

(2) We do not consider the deformation role played by the entanglements which concentrate in the amorphous regions.

(3) We do not consider structural changes that may occur within the crystalline regions.

We nevertheless expect to obtain valuable information on the behaviour of the system. Whenever the resulting distribution of segments is nonuniform, a distribution of weighting factors p_i results from equation (7) and a selfconsistent density is to be formed via iterations. The free energy of the system is discussed in Appendix A.

As will be clear to the reader, we can model numerous interesting phenomena. Only a selection of our results are presented in this paper. We used a relatively small system, $M = 10$, $r = 100$ and a $\phi^{melt} = 0.95$, on a cubic lattice to demonstrate interesting deformation properties. The gambler's ruin analysis discussed previously was used to calculate the chain population for the amorphous phase of an instantly melt-crystallized polymer. Since $r \gg M$, floating chains are almost absent. Therefore we decided to treat our system as closed (i.e., no mass transfer). No floating chains can diffuse in or out of the system. We also like to limit our analysis to totally flexible chains and therefore, we will not examine temperature effects. Another assumption we are incorporating into our system is that any bridges which were fully elongated during deformation are randomly changed into 1 or 2 cilia. There is one interesting parameter whose value is left to choice: the interaction parameter χ. The value for this parameter depends on the polymer, but it is always very high, $\chi \gg \chi_\theta$. This can be shown to be intuitively correct by pointing out that the melt, which is in equilibrium with the air, has an extremely high density. In other words there is a phase transition, air–polymer, therefore $\chi > \chi_\theta$. Unfortunately, for very high χ values, the calculations are very difficult. To understand the properties of our system we must study its behaviour for different χ values. One can imagine that we replace the holes by solvent molecules which lowers the χ value. This step of convenience will as a side benefit give us insight into the swelling behaviour of the system. For $r = 100$, the $\chi_\theta \cong 0.6$. *Figures 7a* and *7b* show the density profile during deformation for $\chi = 0$ and $\chi = 1$ respectively. The difference between *Figures 7a* and *7b* is a remarkable one. When $\chi < \chi_\theta$, the density profile is relatively flat whilst when $\chi > \chi_\theta$ there is a greater variation and necking takes place at higher wall separations. The higher the χ value the more profound the necking process. (The broken curves in *Figure 7b* are less accurate).

Firstly we will discuss the birefringence predictions. *Figure 8a* shows the total fraction of bonds parallel to the surfaces, f^{par}, as a function of the deformation ΔM for various χ values. As in *Figure 7*, there is again a remarkable difference in the curves for $\chi < \chi_\theta$ and $\chi > \chi_\theta$. For $\chi < \chi_\theta$ the curves decrease monotonically, while for $\chi > \chi_\theta$ there is a minimum in the curve. This minimum represents the wall distance at which necking begins. The higher the χ value the smaller ΔM to find this minimum distance. How can this minimum be explained? The unperturbed amorphous region had no net orientation. As soon as deformation begins, the chains are stretched and the number of segment bonds parallel to the surfaces must therefore decrease. When the interaction parameter is weak, $\chi < \chi_\theta$, this process will continue until the system breaks, but when the interactions are strong, $\chi > \chi_\theta$, the introduction of holes (or solvent) into the system is very

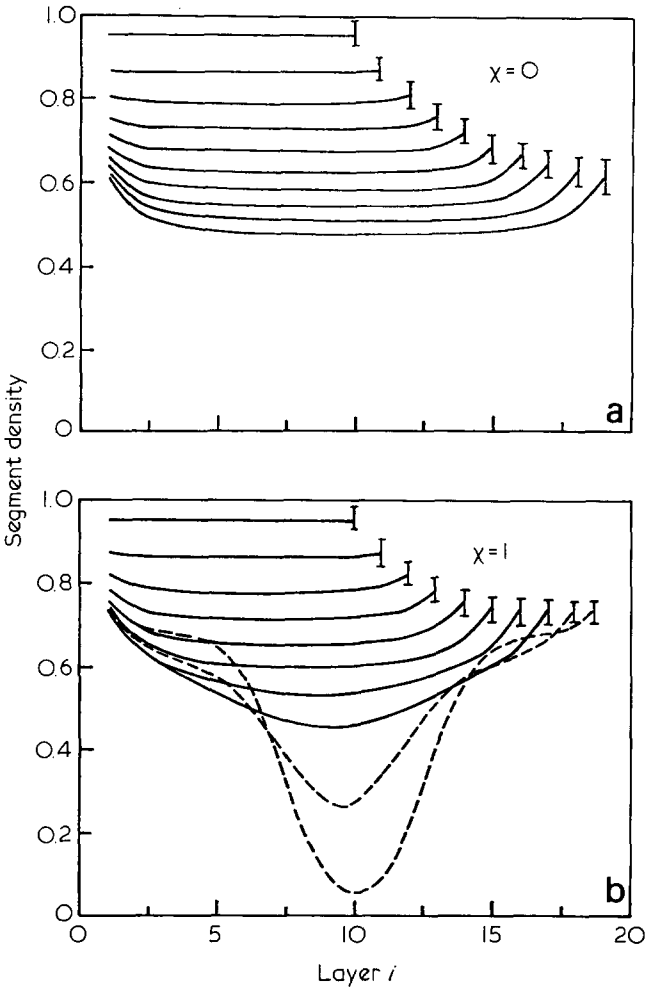

Figure 7 Deformation of the amorphous phase of a semicrystalline polymer. The density profile for different wall distances (indicated by the vertical lines) is shown for (a) athermal solution, (b) $\chi > \chi_0$ ($\chi = 1$) [The broken lines may have an error of a few %]

unfavourable! Therefore the chains tend to have a high density near the walls and a low density in the centre. This is an active response of the chains to the deformation and again results in a higher number of segment bonds parallel to the surfaces. *Figure 8b* shows the free energy as a function of deformation for different χ values. We see that the curves for high χ values level off faster than for low χ values. Therefore, the high χ value curves probably start off steeper than the low χ value curves, indicating that the material is harder to deform. At low χ values (good solvents) the system is much more elastic in character and the material becomes soft. Whan happens to the free energy after necking starts is not known.

To illustrate the individual behaviour of loops, bridges, cilia and floating chains during deformation, we have plotted the density profiles for three wall distances in *Figure 9*: $M = 10$ (unperturbed), $M = 15$ (just before necking) and $M = 19$ (after necking). *Figure 9* is for the case $\chi = 1$, but we note that the behaviour of the chain for all χ values up to the start of necking during deformation is more or less the same.

Figure 9a shows that the loops are almost inactive. This is because most of the loops are very small. All the other chains are more deformationally active. Since necking occurs when $M = 19$, all of the chains must have a dip in their density profiles. The most profound change in the density profile is found for the floating chains. They desert the centre region completely and choose one of the two sides of the system. Bridges must cross the centre of the system, and therefore they do not display a similar change in their profile (*Figure 9b*). They will however, show a deeper dip in the profile in systems where more (longer) bridges are present.

Cilia react upon deformation by retracting in their tails. In the $M = 19$ system, the cilia hardly ever cross the centre of the system.

The most important conclusion from our deformation calculations is that the deformation of the amorphous phase is more energetically than entropically controlled. We saw that at very high χ value a necking process sets in at small deformations.

CONCLUSIONS

For an instaneous melt crystallization process, we are able to analyse the amorphous phase of a semicrystalline polymer system in terms of the gambler's ruin analysis for chains of finite length. It appears that a large fraction of the segments belong to cilia and floating chains, even for a rather high molecular weight polymer. By incorporating chain stiffness into the model we see that backfolding can alter our results significantly, but the principle of rescaling

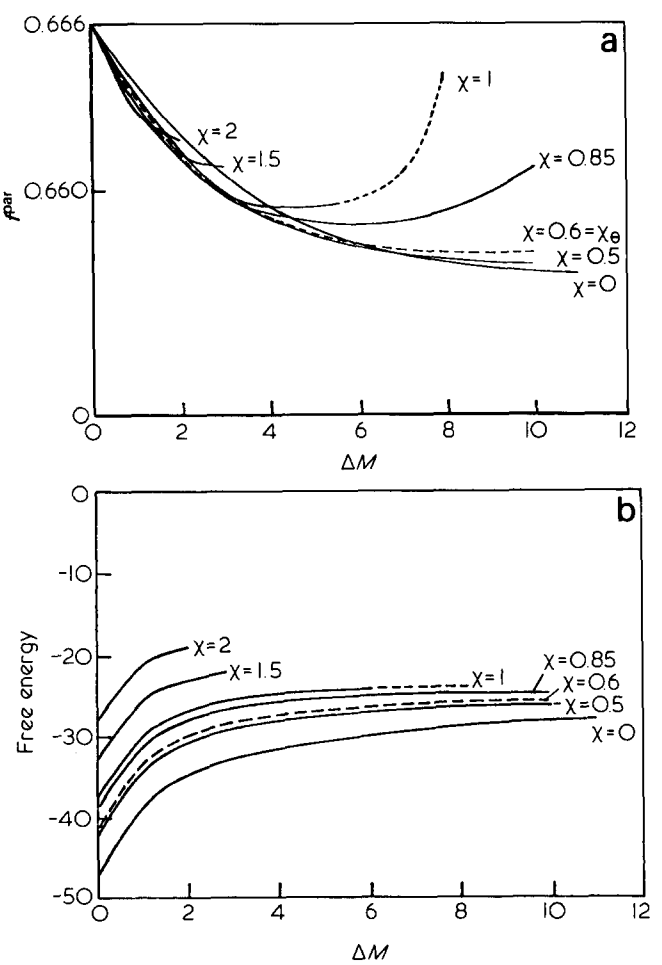

Figure 8 (a) Birefringence behaviour during the deformation. Total fraction of bonds parallel to the surfaces is plotted against the ΔM for different χ values. (b) Free energy behaviour during the deformation for different χ values

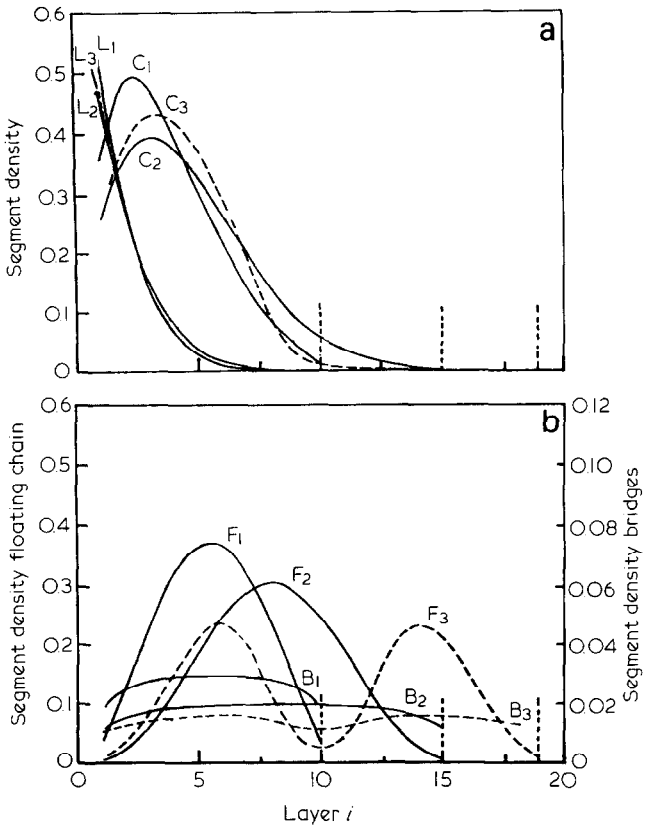

Figure 9 Individual response of the chain species on deformation, for (1) $M=10$; (2) $M=15$; (3) $M=19$. (Again there can be a small error for $M=19$) (a) Profile for the loops, L, and cilia, C, given for one wall. (b) Profile for the bridges, B, from both walls (right hand axis) and that for floating chains, F (left hand axis)

of statistical chain elements nearly compensates for the differences. In studying deformation we find that it is energetically rather than entropically controlled. We find $\chi > \chi_\theta$ values caused a necking process while low χ values (swelling) make the material soft and flexible.

APPENDIX A

Free energy in melt and amorphous phase

As a final result of self consisting computer calculations, the free energy, interaction energy and entropy can be evaluated. Scheutjens and Fleer (SF) derive the free energy from their canonical function $Q(M, L, T, \{n_c\})$ for an arbitrary but specified set of conformations $\{n_c\}$. Their analysis is for a polymer system in equilibrium with a bulk solution. The SF result is:

$$-\frac{F}{kTL}=\frac{n}{L}\ln\phi_* + \sum_{i=1}^{M}(\phi_i^0 \ln \phi_i^0 - \phi_i \ln p_i) + U/kTL \quad (A1)$$

where U/kTL is the interaction energy given by:

$$U/kTL=\chi \sum_{i=1}^{M} \phi_i\langle\phi_i^0\rangle - \chi_s(\phi_1+\phi_M) \quad (A2)$$

and ϕ_* is the volume fraction far away from the walls (bulk). While $\phi_*=(rn/Lp(r))$, equation (A1) can be re-written for a closed system.

$$-\frac{F}{kTL}=\frac{n}{L}\ln\frac{rn}{Lp(r)} + \sum_{i=1}^{M}(\phi_i^0 \ln \phi_i^0 + \phi_i \ln p_i) + U/kTL \quad (A3)$$

When $\chi_s=0$ and when reflecting boundaries are used, equation (A3) is the free energy for an M-layer melt system. Let us now examine the first term of equation (A3) closely. Clearly this is the important term for the amorphous phase. We write

$$\frac{n}{L}\ln\frac{rn}{Lp(r)}=\frac{n}{L}\ln\frac{n}{Lp(r)}+\frac{n}{L}\ln r \quad (A4)$$

The last term in (A4) is a normalization term. The first term is more interesting. The argument $(n/Lp(r))$ is the quotient of: the number of chains per lattice site divided by the probability of finding an r-mer in the system. In the melt $p_i=1$, $p(r)=M$ and $(n/Lp(r))=n/LM$. Realizing that the free energy for our amorphous phase and the identical portion of the melt must be the same and

$$\left(\frac{nr}{L}\right)^{\text{melt}}=\left(\frac{n^{\text{free}}r}{L}+\sum_s s\left[\frac{n_s^{\text{loop}}}{L}+\frac{n_s^{\text{bridge}}}{L}+\frac{n_s^{\text{cilium}}}{L}\right]\right)^{\text{amorphous phase}} \quad (A5)$$

because of the conservation of segments, leads to the following formula for the free energy for the amorphous phase of a semicrystalline polymer system:

$$\begin{aligned}\frac{F}{kTL}=&\frac{n^{\text{free}}}{L}\ln\frac{n^{\text{free}}}{Lp(\text{free})}\\ &+\sum_s\frac{s}{r}\left[\frac{n_s^{\text{loop}}}{L}\ln\frac{n_s^{\text{loop}}}{Lp(\text{loop},s)}\right.\\ &+\frac{n_s^{\text{cilium}}}{L}\ln\frac{n_s^{\text{cilium}}}{Lp(\text{cilium},s)}\\ &\left.+\frac{n_s^{\text{bridge}}}{L}\ln\frac{n_s^{\text{bridge}}}{Lp(\text{bridge},s)}\right]\\ &+\frac{n}{L}\ln r+\sum_{i=1}^{M}(\phi_i^0\ln\phi_i^0+\phi_i\ln p_i)+U/kTL \quad (A6)\end{aligned}$$

where

$$p(\text{free})=\sum_{i=1}^{M} p^{\text{f}}(i,r) \quad (A7)$$

$$p(\text{loop},s)=p^{\text{c}}(1,s)\lambda_{-1}\lambda_1(r-s-1)*2 \quad (A8)$$

$$p(\text{cilium},s)=p^{\text{f}}(1,s)*\lambda_1*2*2 \quad (A9)$$

$$p(\text{bridge},s)=p^{\text{c}}(M,s)*\lambda_{-1}\lambda_{-1}(r-s-1)*2 \quad (A10)$$

In (A8–A10) we added extra factors of 2 to account for both walls (see equations (15), (16), (18), (19)). It is easy to check that, as long as the amorphous phase is unperturbed, equations (A6) and (A3) give the same results. During deformation, the number of chainparts will be constant, only the p-values in equation (A6) will change.

Finally we examine temperature effects on the free energy expression. Analogous to the discussion above we can replace the first terms in (A6) by:

$$\frac{n^{\text{x}}}{L}\ln\frac{n^{\text{x}}}{Lp(\text{x})^{T_i}} \quad \text{etc.} \quad (A11)$$

where x stands for a specified chain species. The superscript T_1 is the current temperature. Again when the temperature changes, the reference number of chain species x in the argument will remain constant.

APPENDIX B

Computational tricks

Many calculations can be optimized. We will briefly discuss two of the most important tricks. The volume fractions are calculated by:

$$\phi_i = \sum_{s=1}^{r} \text{norm}(s) \sum_{k=s}^{r} p(i,k)p(i,s-k+1) \qquad \text{(B1)}$$

While $p(i,s-k+1)=0$ if $k>s$, the summations can be rearranged:

$$\phi_i = \sum_{s=1}^{r} \sum_{k=s}^{r} p(i,s)\,\text{norm}(k)p(i,k-s+1) \qquad \text{(B2)}$$

or:

$$\phi_i = \sum_{s-1}^{r} p(i,s)p^{\text{inv}}(i,r-s+1) \qquad \text{(B3)}$$

The $\underline{\underline{p}}^{\text{inv}}$ matrix can now be calculated by the recurrence relation:

$$p^{\text{inv}}(i,s) = p_i[\lambda_{-1}p^{\text{inv}}(i-1,s-1) + \lambda_0 p^{\text{inv}}(i,s-1) + \lambda_1 p^{\text{inv}}(i+1,s-1) + \text{norm}(r-s+1)] \qquad \text{(B4)}$$

This reduces the number of calculations significantly.

Secondly, the stiffness calculations can be reduced. As can be proven by induction, the 6×6 matrices can be replaced by 3×3 matrices, while bonds in the plane are indistinguishable. So equation (25) and (29) can be replaced by:

$$\lambda_{-1} = \begin{vmatrix} S & 4L & B \\ 0 & 0 & 0 \\ 0 & 0 & 0 \end{vmatrix} \qquad \lambda_0 = \begin{vmatrix} 0 & 0 & 0 \\ L & 2L+B+S & L \\ 0 & 0 & 0 \end{vmatrix}$$

$$\lambda_{+1} = \begin{vmatrix} 0 & 0 & 0 \\ 0 & 0 & 0 \\ B & 4L & S \end{vmatrix} \qquad \text{(B5)}$$

$$\underline{\underline{w}}'_{\text{sub}} = \begin{vmatrix} B & 4L & S \\ L & 2L+B+S & L \\ S & 4L & B \end{vmatrix} \qquad \text{(B6)}$$

The direction in the plane is four fold degenerated. This has some consequences for the volume fraction calculations.

REFERENCES

1 Pettracone, V., Sanchez, I. C. and Stein, R. S. *J. Polym. Sci., Polym. Phys. Edn.* 1975, **13**, 1981
2 Lohse, D. J. and Gaylord, R. J. *Polym. Eng. Sci.* 1978, **18**, 512
3 DiMarzio, E. A. and Rubin, R. J. *J. Chem. Phys.* 1971, **55**, 4318
4 Gaylord, R. J. and Lohse, D. J. *J. Chem. Phys.* 1978, **65**, 2778
5 Lohse, D. J. and Gaylord, R. J. *J. Chem. Phys.* 1977, **66**, 3842
6 Flory, P. J. and Yoon, D. Y. *Nature* 1979, **272**, 226
7 Guttman, C. M., DiMarzio, E. A. and Hoffman, J. D. *Polymer* 1980, **21**, 733
8 Guttman, C. M., DiMarzio, E. A. and Hoffman, J. D. *Polymer* 1981, **22**, 1466
9 Rubin, R. J. see acknowledgement in ref. 7
10 Scheutjens, J. M. H. M. and Fleer, G. J. *J. Phys. Chem.* 1979, **83**, 1619
11 Scheutjens, J. M. H. M. and Fleer, G. J. *J. Phys. Chem.* 1980, **84**, 178
12 Levine, S., Thomlinson, M. M. and Robinson, K. *Disc. Faraday Soc.* (1978), **65**, 202
13 Gaylord, R. J., Paisner, M. J. and Lohse, D. J. *Macromol. Sci. Phys.* 1980, **B17**, 473
14 Mansfield, M. L. *Macromolecules* 1983, **16**, 914
15 Guttman, C. M. and DiMarzio, E. A. *Macromolecules* 1982, **15**, 525